Article

Achievable Rate of NOMA-Based Cooperative Spectrum-Sharing CRN over Nakagami-*m* Channels

Sajid Hussain Alvi [1], Bakhtiar Ali [2], Jawad Mirza [2], Ali Khaqan [2], Muhammad Awais Javed [2], Jehad Ali [3] and Niamat Hussain [4],*

[1] Department of Physics, COMSATS University, Islamabad 45550, Pakistan
[2] Department of Electrical and Computer Engineering, COMSATS University, Islamabad 45550, Pakistan
[3] Department of Computer Science and Engineering, Sejong University, Seoul 05006, Republic of Korea
[4] Department of Smart Device Engineering, Sejong University, Seoul 05006, Republic of Korea
* Correspondence: niamathussain@sejong.ac.kr

Abstract: Efficient data dissemination is a key challenge for IoT applications. In this paper, we present an ergodic achievable rate analysis of the non-orthogonal multiple access (NOMA)-based cooperative transmission scheme in spectrum-sharing cognitive radio networks (CRNs). The transmission scheme consists of two phases, where the NOMA transmission strategy is employed at the secondary transmitter (ST) in the second phase to serve the primary receiver (PR) and secondary receivers (SRs). This cooperative spectrum-sharing transmission is favourable when the ST-PR link is strong and the ST faces a spectrum scarcity issue. To evaluate the performance of the network over Nakagami-*m* channels, ergodic achievable rates at PR and SRs are derived in closed forms, which can be used for any integer or non-integer value of fading index *m*. Finally, we compare the results of the analytical expressions with simulated results for validation.

Keywords: non-orthogonal multiple access (NOMA); cognitive radio; achievable rate; Nakagami-*m* channels

1. Introduction

The Internet of Things (IoT) is considered to be a useful component of future smart cities and provides several new applications for human safety and comfort. Physical devices are embedded with small sensors that help collect data from the devices itself as well as their surroundings. These data are transmitted to remote servers for analyses and feedback. So, the major benefit of IoT in future networks will be in the form of providing connected physical devices [1].

The efficient sharing of an available spectrum is considered to be a challenging task in IoT networks. The lack of spectrum and power resources in IoT networks limits their performance. To overcome this performance limitation, the introduction of collaborative communication with the support of cognitive radio technologies is believed to be essential [2,3]. The allocation of spectrum bands to IoT devices is regarded as a non-trivial task since the number of IoT devices is predicted to increase significantly in future. Thus, it is important to design spectrum-sharing techniques for future IoT networks.

In addition to cooperative spectrum sharing among networks, efficient multiple access techniques are also essential for achieving effective spectrum utilization. In this regard, it is expected that the role of non-orthogonal multiple access (NOMA) will be important as it can help improve spectral efficiency gains compared to conventional orthogonal multiple access (OMA) schemes [4–6]. More precisely, NOMA allows users to use the same time/frequency resource but with different power levels. The users employ successive interference cancellation (SIC) techniques to get rid of co-channel interferences and obtain the desired message. It has been shown in the literature that when NOMA is integrated

with cognitive radio networks, the network's performance improves in terms of spectral efficiency and connectivity [7].

In IoT-based future communication networks, there will be a massive number of devices that will compete among each other for the spectrum resource. In order to meet their spectrum requirements, IoT devices may have to collaborate with the devices of the surrounding networks. In this study, we consider a cognitive radio spectrum-sharing network, where two set of users are present: primary users (PUs) and secondary users (SUs). The PUs are the licensed owners of the frequency band, whereas the SUs are the unlicensed users (IoT devices). By allocating the licensed spectrum of the PU to the unlicensed SU, cognitive radios can increase the spectral efficiency of a communication system [8]. A cognitive radio can operate in three different ways, namely, interweave, overlay, and underlay spectrum-sharing paradigms [8]. NOMA can be used in spectrum-sharing cognitive radio networks to meet the higher spectral efficiency and high connectivity requirements of future wireless networks [7]. More precisely, NOMA-based cooperative spectrum-sharing networks can improve the reception's reliability (i.e., lower outage probability) compared to their non-cooperative counterparts [4].

2. Related Work

For a NOMA-based cognitive radio network (CRN) in an underlay spectrum-sharing scenario, a closed-form study of the average achievable sum rate and outage probability was taken into consideration in [9]. The authors took into account the peak interference restriction, which states that the secondary network's interference on the primary user's receiver must be below a specific threshold. They demonstrated that at high values of peak interference power at the PU-Rx, the CRN-NOMA outperforms the CRN with the standard OMA [9]. In contrast, the same authors proposed a system in which the secondary user's receiver and the relay both have multiple receive antennas and employ selection combining and maximal-ratio combining (MRC) to receive signals [10]. The average achievable rate and outage probabilities for the spectrum-sharing-based cooperative NOMA are determined using closed-form equations.

The authors in [11] presented a scheme in which the secondary base station would send a power domain NOMA signal to the closest secondary user after detecting an idle channel. The first secondary user uses a decode-and-forward approach to send the signal meant for the second secondary user in addition to deciphering its own signal. The authors combined the design and analysis of the proposed strategy, as opposed to other publications that tackled the spectrum-sensing and transmission phases separately [11]. Analytical equations for the outage probability and the ergodic rate of the two secondary users were derived to show the performance of the latter by assuming a flat Rayleigh fading channel model. In [12], the channel condition between the primary transmitter and receiver is assumed to be weak, and a secondary transmitter is used to assist the primary transmitter while simultaneously transmitting in a full-duplex mode to a secondary receiver with strong channel conditions. Zero-forcing beamforming is implemented at the secondary transmitter to suppress self-interferences. The outage probabilities for primary and secondary networks are also derived in [12]. According to a peak interference constraint, the authors in [13] derived analytical formulas for the sum effective rate for the downlink NOMA system. They explored the way the system's performance was affected by the availability of various degrees of channel state information (instantaneous and statistical). Other important factors were taken into consideration, and their effects on the system's sum effective rate were investigated. These factors included the maximum tolerated interference level, the delay exponent, the number of antennas, and the number of users. In [5], a cooperative NOMA transmission scheme is proposed, which is based on user pairing. Therein, it is reported that when users with distinctive channel gains are paired together, then the performance gain of the cooperative NOMA scheme over the OMA scheme is large. Furthermore, the performance analysis of the cooperative NOMA scheme proposed in [5] is also presented in terms of outage probability and diversity order.

In [14], the authors investigated NOMA in multicast CRNs, where the multicast secondary users function as relays to improve the performance of both primary and secondary users. Closed-form expressions for outage probability and diversity order were also derived in [14]. The performance analysis of NOMA-based CRNs was performed in [15], where closed-form expressions are derived for outage and throughput. An underlaying NOMA CRN with detect-and-forward processes was investigated in [16], where a closed-form outage probability expression for NOMA-assisted secondary users was derived. A NOMA-based cognitive hybrid satellite-terrestrial overlay network was studied in [17] using amplify-and-forward (AF) relaying mode. Therein, the authors derived closed-form outage probability expressions for primary and secondary users.

In addition to the half-duplex transmission, the statistical performance characterization of NOMA-based CRNs with full-duplex transmission also received substantial attention [6,18–20]. In [18], the full-duplex mode of transmission is used at a double antenna relay to support multiple cell-edge users and to achieve a high throughput. To overcome interferences in the system, the source-to-relay and relay-to-destination transmission phases are carried out in licensed and unlicensed bands, respectively. Moreover, in [18], the performance of the system is characterized in terms of outage probabilities and ergodic sum rates. In [19], the performance of a NOMA system is improved by transforming one of the user (with a good channel condition) into a full duplex relay. For such a system, the authors in [19] also derived a simple achievable rate region. A full-duplex based device-to-device (D2D) cooperative NOMA transmission strategy was proposed in [6], where strong NOMA users support weak NOMA users. Therein, an adaptive multiple access method was also investigated in [6], where depending on the residual self interference level, the system switches between a cooperative NOMA and conventional NOMA and OMA schemes. This dynamic multiple access method yields the best outage performance. The outage probability expression of the system was also derived in [6]. A downlink NOMA system with cooperative relaying was studied in [20], where the users near the base-station act as full-duplex relays for users that are far from the base station. Closed-form expressions for outage probability and ergodic sum rate were also presented in [20].

Most existing studies on the performance characterization of half-duplex NOMA-based CRNs assume Rayleigh fading channels. A cooperative spectrum-sharing protocol based on NOMA to protect the quality of service of cell-center primary users, in which the secondary transmitter works with the primary to attain full rates via cooperative multiplexing, was considered in [21]. They derived closed-form expressions for the average bit error rate and evaluated the performance of primary users. A cooperative NOMA-based spectrum-sharing system was introduced in [7], where the primary network shares the spectrum with the secondary network. In exchange, the secondary network transmits the messages of the primary and secondary networks using NOMA. The proposed scheme is useful when the secondary transmitter has better channel conditions relative to the primary receiver but lacks the radio spectrum. To obtain better insights of the system, it is useful to extend the analysis of the system to the ergodic achievable rate with arbitrary values of fading parameter m.

In this study, we derive ergodic achievable rate expressions for NOMA-based cooperative spectrum-sharing CRNs over Nakagami$-m$ fading channels. For our performance analyses, we use the same system model and channel model as those in [7], where the authors derived outage probability expressions for both primary and secondary users. In contrast to [7], here, we provide the ergodic capacity analysis for primary and secondary users in the NOMA-based cooperative spectrum-sharing CRN. The derived analytical achievable rate expressions presented in this paper provide some insights with respect to how the system's performance is affected under different fading severity and NOMA power levels. The contributions of this study are summarized below:

- For the cooperative NOMA-based spectrum-sharing system, assuming the Nakagami-m fading channel model, we derive the exact closed form expressions of the ergodic sum rate for both primary and secondary users.

- The ergodic sum rate expressions derived in this paper are comprehensive as they are valid for any integer or non-integer values of the Nakagami-*m* fading severity parameter.

The performance analysis presented in this study assists in predicting the performance of NOMA-based CRNs for various propagation conditions, such as line-of-sight (LoS) or non-line-of-sight (NLoS) conditions. These propagation conditions can be attained by varying the fading severity parameter, *m*, in Nakagami-*m* fading channels. Another useful application of these derived expressions is that the transmission power's optimization can be performed on NOMA-based CRNs where the knowledge of instantaneous channel state information (CSI) is not available at the transmitter.

The paper is organized as follows. Section 3 describes the system's model of the NOMA-based cooperative CRN. Section 4 presents the achievable rate analysis of both primary and secondary users. Section 5 provides a discussion on the numerical results. Finally, Section 6 presents the conclusions of the paper.

3. System Model

Consider the cooperative spectrum-sharing network shown in Figure 1, which consists of a primary transmitter (PT) who is a licensed user possessing their own frequency spectrum, a secondary transmitter (ST) who does not have any spectrum of their own to transmit its signal, and a primary (licensed) receiver (PR) and *K* secondary (unlicensed) receivers (SRs). There are two networks that can be classified as primary and secondary networks. In our model, the secondary network consisting of IoT devices cooperates with the primary network to transmit their messages, but IoT devices also help relay the message of the primary network. From this point onward, we represent the IoT transmitter and receivers as ST and SRs, respectively. The cooperative spectrum-sharing transmission strategy is divided into two phases. In the first transmission phase, only the PT is allowed to transmit the message to the PR, whereas, in the second transmission stage, ST uses the NOMA technique to transmit the signals to both PT and SRs.
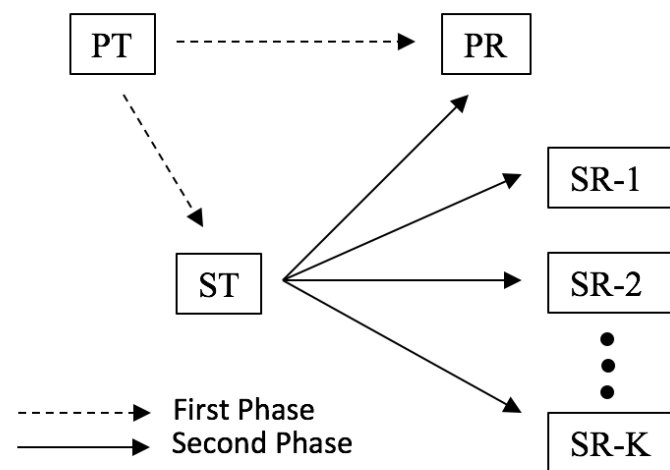

Figure 1. A depiction of a NOMA-based spectrum-sharing CRN with two transmission phases.

3.1. Received Signals in Two Transmission Phases

Each node (transmitter/receiver) consists of a single antenna, and half duplex transmission is assumed. Similarly to [7], the cooperative NOMA-based transmission has two phases. In the first phase, the PT sends a symbol, x_0, to the PR with transmission power, P_p, such that the PR receives

$$y_p^{(1)} = \sqrt{P_p} h_p x_0 + n_p^{(1)}, \tag{1}$$

where h_p denotes the channel between the PT and PR. $n_p^{(1)}$ is the noise term in the first transmission phase at the PR, which is assumed to follow a Gaussian distribution with zero-mean and variance σ_p^2. During the first transmission phase, the same symbol, x_0, is also received at ST and SRs, where the received signals at ST and SRs can be expressed as

$$y_s^{(1)} = \sqrt{P_p} h_s x_0 + n_s^{(1)} \tag{2}$$

and

$$y_{s,k}^{(1)} = \sqrt{P_p} h_{s,k} x_0 + n_{s,k}^{(1)} \tag{3}$$

respectively, and h_s denotes the channel between the PT and ST; $h_{s,k}$ represents the channel between the PT and k^{th} SR. $n_s^{(1)}$ and $n_{s,k}^{(1)}$ denote the noise terms at the ST and k^{th} SR, which are assumed to follow Gaussian distributions with zero means and variances σ_s^2 and $\sigma_{s,k}^2$, respectively. Here, we assume that $\sigma_p^2 = \sigma_s^2 = \sigma_{s,k}^2$, $\forall k$. The ST successfully decodes symbol x_0, when $\rho_p |h_s|^2 \geq 2^{2R_0} - 1$, where R_0 is the target data rate of PR and $\rho_p = P_p / \sigma_s^2$.

Once symbol x_0 is successfully decoded at the ST in the first transmission phase, the ST superimposes this symbol with the symbols of SRs for the next NOMA-based transmission phase. The superimposed signal generated at the ST is given by $\sqrt{\alpha_0 P_s} x_0 + \sum_{k=1}^{K} \sqrt{\alpha_k P_s} x_k$, where x_k is the symbol of the kth SR, and P_s represents the transmission power at the ST. This superimposed signal is transmitted from the ST to PR and SRs in the second transmission stage. Therefore, the received signals at the PR and k^{th} SR in the second transmission phase are given by

$$y_p^{(2)} = g_p \sum_{i=0}^{K} \sqrt{\alpha_i P_s} x_i + n_p^{(2)} \tag{4}$$

and

$$y_{s,k}^{(2)} = g_{s,k} \sum_{i=0}^{K} \sqrt{\alpha_i P_s} x_i + n_{s,k}^{(2)} \tag{5}$$

respectively, where g_p denotes the channel between ST and PR in the second transmission phase. Similarly, $g_{s,k}$ represents the channel between the ST and k^{th} SR. $n_p^{(2)}$ and $n_{s,k}^{(2)}$ are noise terms at the PR and the kth SR, respectively, in the second transmission phase, which are assumed to follow Gaussian distributions with zero mean and the same variances as in the first transmission stage.

3.2. Achievable Rates at PR and SRs

The PR applies MRC on the received signals of two phases, and the achievable data rate (in bits per second (bps)) at the PR can be expressed as

$$R_p^{\text{NOMA}} = \frac{1}{2} \log_2 \left(1 + \rho_p |h_p|^2 + \frac{\rho_s |g_p|^2 \alpha_0}{\rho_s |g_p|^2 \sum_{i=1}^{K} \alpha_i + 1} \right). \tag{6}$$

where $\rho_s = P_s / \sigma_s^2$. On the other hand, the achievable data rate (in bps) at the kth SR is given by

$$R_{s,k}^{\text{NOMA}} = \frac{1}{2} \log_2 \left(1 + \frac{\rho_s |g_{s,k}|^2 \alpha_k}{\rho_s |g_{s,k}|^2 \sum_{i=k+1}^{K} \alpha_i + 1} \right). \tag{7}$$

The achievable data rate (in bps) of the last secondary user is provided as follows; i.e., the user K can be expressed as

$$R_{s,K}^{\text{NOMA}} = \frac{1}{2} \log_2 \left(1 + \rho_s |g_{s,K}|^2 \right) \tag{8}$$

However, if the ST fails to decode x_0, there will be no NOMA-based transmissions in the second stage. The achievable data rate (in bps) at the PR then becomes

$$R_p^{\text{ST-silent}} = \frac{1}{2} \log_2\left(1 + \rho_p |h_p|^2\right) \tag{9}$$

and the achievable rate at the SR is zero, i.e., $R_{s,k}^{\text{ST-silent}} = 0 \ \forall k$. This is due to the fact that the ST can use the resource of the PT only if it can improve or maintain the rate of the PT. Therefore, if it fails to decode x_0 transmitted by this particular PT, it cannot transmit the symbols to its respective SRs in the next time slot.

The SIC is implemented at the kth SR to separate the superimposed signals in the power domain. In particular, the kth SR detects the symbol of the jth SR, where $j < k$, which is then removed from the received signal in a successive manner, whereas, if $j > k$, then the jth SR symbol is treated as noise at k^{th} SR. Therefore, we can write the achievable data rate for k^{th} SR to detect the symbol of the primary receiver ($j = 0$) as

$$R_{0,k} = \frac{1}{2} \log_2\left(1 + \rho_p |h_{p,k}|^2 + \frac{\rho_s |g_{s,k}|^2 \alpha_0}{\rho_s |g_{s,k}|^2 \sum_{i=1}^{K} \alpha_i + 1}\right).$$

where $h_{p,k}$ is the channel between the PT and the kth SR. The achievable data rate for k^{th} SR to detect the symbol of the jth SR, where $1 \le j \le k$, is given by

$$R_{j,k} = \frac{1}{2} \log_2\left(1 + \frac{\rho_s |g_{s,k}|^2 \alpha_j}{\rho_s |g_{s,k}|^2 \sum_{i=j+1}^{K} \alpha_i + 1}\right). \tag{10}$$

Note that symbol x_j can be decoded and removed by the kth SR, if $R_{j,k} \ge R_j$, where R_j is the target data rate of the jth SR. This successive cancellation process continues until x_k is successfully decoded at the kth SR.

4. Achievable Rate Analysis

For achievable sum rate analyses, we assume that all wireless communication links (i.e., h_p, h_s, $h_{s,k}$, g_p, and $g_{s,k}$) experience Nakagami-m fading. Here, we derive the average sum rate of the NOMA-based spectrum-sharing network discussed in the previous section. First, we provide a preliminary analysis of the Nakagami-m-distributed channels in a point-to-point wireless communication system. Then, we present our ergodic achievable rate analyses of the network.

4.1. Preliminaries

Let h denote the Nakagami-m-distributed fading channel coefficient with the probability density function (PDF) as ([22], Equation (5.35))

$$f_h(h) = \frac{2m^m h^{2m-1}}{\Omega^m \Gamma(m)} exp\left(-\frac{mh^2}{\Omega}\right), \quad h \ge 0, \tag{11}$$

where $m \ge 0.5$ is the fading severity parameter, $\Gamma(\cdot)$ is the Gamma function ([23], Equation (8.310.1)), and $\Omega = \mathbb{E}\{|h|^2\}$. Nakagami-$m$ distribution is generally used to model fading scenarios with one strong, i.e., line-of-sight (LoS), and many weaker, i.e., non line-of-sight signal, components. This distribution approximates the fading channel's coefficient of a vector process where the central limit theorem may not be necessarily valid. Moreover, when the fading channel coefficient of a certain link is Nakagami-m-distributed, then the instantaneous SNR for the corresponding link is gamma-distributed. The PDF of the instantaneous SNR can then be written as ([22], Equation (5.37)).

$$f_\gamma(\gamma) = \frac{m^m \gamma^{m-1}}{\overline{\gamma}^m \Gamma(m)} exp\left(-\frac{m\gamma}{\overline{\gamma}}\right), \quad \gamma \geq 0 \tag{12}$$

where $\gamma = \frac{P}{\sigma^2}|h|^2$ is the instantaneous SNR, and $\overline{\gamma} = \frac{P}{\sigma^2}\Omega$ is the average SNR. It may be noted that P denotes the transmit power whereas σ^2 represents the variance of the zero mean Gaussian thermal noise added at the receiver. This PDF expression can alternatively be written in terms of Fox's H-function as ([24], Equation (2)).

$$f_\gamma(\gamma) = \frac{\left(\frac{m}{\overline{\gamma}}\right)}{\Gamma(m)} H^{1,0}_{0,1}\left[\frac{m\gamma}{\overline{\gamma}} \middle| \begin{array}{c} \overline{} \\ (m-1,1) \end{array}\right], \tag{13}$$

where $H^{m,n}_{p,q}[\cdot]$ is the Fox's H-function represented by Mellin–Barnes-type integrals and is defined as ([25], Equation (1.1.1)). Fox's H-function is a generalized function in the sense that most special functions of one variable can be represented in terms of this function. It has applications in various problems arising in engineering, physical sciences, and statistics [25].

When the transmitter does not have knowledge of the channel state information (CSI), then it can not adapt its power in accordance to CSI. It is then feasible for the transmitter to operate with constant power. Therefore, the ergodic capacity of the fading channel is obtained by averaging over the SNR distribution and is defined as ([22], Equation (14.74)).

$$\bar{R} := \frac{1}{2}\int_0^\infty \log_2(1+\gamma) f_\gamma(\gamma)\, d\gamma, \tag{14}$$

where factor $\frac{1}{2}$ is a result of the two transmission phases. For mathematical convenience, function $log_2(1+\gamma)$ in (14) can be expressed in terms of Fox's H-function ([26], Equation (2.4.3)). This representation of $log_2(1+\gamma)$ will facilitate us in the upcoming calculations.

$$\log_2(1+\gamma) = \frac{1}{\ln(2)} H^{1,2}_{2,2}\left[\gamma \middle| \begin{array}{c} (1,1),(1,1) \\ (1,1),(0,1) \end{array}\right]. \tag{15}$$

4.2. Ergodic Achievable Rates

Ergodic Achievable Rate at the PR: Using the instantaneous achievable data rate at the PR (6), the associated ergodic achievable data rate at the PR can then be written as

$$\bar{R}^{\text{NOMA}}_p = \mathbb{E}\{R^{\text{NOMA}}_p\} = \frac{1}{2}\mathbb{E}\left\{\log_2\left(1+\gamma_p+\frac{\gamma_s\,\alpha_0}{\gamma_s\,\alpha+1}\right)\right\}, \tag{16}$$

where $\gamma_p = \rho_p|h_p|^2$, $\gamma_s = \rho_s|g_p|^2$, and $\alpha = \sum_{i=1}^K \alpha_i$. Expression (16) can be written in an integral form as

$$\bar{R}^{\text{NOMA}}_p = \frac{1}{2}\int_0^\infty \underbrace{\int_0^\infty \log_2\left(1+\gamma_p+\frac{\gamma_s\,\alpha_0}{\gamma_s\,\alpha+1}\right) f_{\gamma_p}(\gamma_p)\, d\gamma_p}_{I}$$

$$\times f_{\gamma_s}(\gamma_s)\, d\gamma_s. \tag{17}$$

Let us first evaluate integral I as

$$I = \int_0^\infty \log_2(1+\gamma_p+C) f_{\gamma_p}(\gamma_p)\, d\gamma_p, \tag{18}$$

where $C = \frac{\gamma_s\,\alpha_0}{\gamma_s\,\alpha+1}$ is used for the sake of simplicity. Now, $\log_2(1+\gamma_p+C) = \log_2(1+\gamma_p) + \log_2\left(1+\frac{C}{1+\gamma_p}\right)$ is expanded and then substituted in (18) to obtain

$$I = \underbrace{\int_0^\infty \log_2(1 + \gamma_p) f_{\gamma_p}(\gamma_p) d\gamma_p}_{I_1}$$

$$+ \underbrace{\int_0^\infty \log_2\left(1 + \frac{C}{1 + \gamma_p}\right) f_{\gamma_p}(\gamma_p) d\gamma_p}_{I_2}. \tag{19}$$

Integral I_1 can be re-written by substituting (13) and (15) in it to obtain

$$I_1 = \frac{\left(\frac{m_0}{\overline{\gamma}_p}\right)}{\ln(2)\Gamma(m_0)} \int_0^\infty H_{2,2}^{1,2}\left[\gamma_p \middle| \begin{array}{c} (1,1),(1,1) \\ (1,1),(0,1) \end{array}\right]$$

$$\times H_{0,1}^{1,0}\left[\frac{m_0\gamma_p}{\overline{\gamma}_p} \middle| \begin{array}{c} \overline{} \\ (m_0-1,1) \end{array}\right] d\gamma_p, \tag{20}$$

where m_0 is the fading parameter for the PT-PR link and $\overline{\gamma}_p = \mathbb{E}\{\gamma_p\}$. The integral in (20) can now be evaluated using ([25], Equation (2.6.8)) to give

$$I_1 = \frac{1}{\ln(2)\Gamma(m_0)} H_{3,2}^{1,3}\left[\frac{\overline{\gamma}_p}{m_0} \middle| \begin{array}{c} (1,1),(1,1),(1-m_0,1) \\ (1,1),(0,1) \end{array}\right]$$

$$= \frac{1}{\ln(2)\Gamma(m_0)} G_{3,2}^{1,3}\left(\frac{\overline{\gamma}_p}{m_0} \middle| \begin{array}{c} 1,\ 1,\ 1-m_0 \\ 1,\ 0 \end{array}\right), \tag{21}$$

where $G_{p,q}^{m,n}(\cdot)$ in the second equality is the Meijer's G-function related to Fox's H-function $H_{p,q}^{m,n}[\cdot]$ via ([25], Equation (1.7.1)). It may be noted that Meijer's G-function is a sub-class of Fox's H-function, and it is relatively simpler to evaluate than compared to Fox's H-function. Another advantage of this function is that there is a built-in function available in most well-known computational software, e.g., MATLAB and MATHEMATICA, etc.

Now, integral I_2 can be rearranged by using identity ([23], Equation (1.511)) as follows.

$$I_2 = \frac{1}{\ln(2)} \sum_{n=1}^\infty \frac{(-1)^{n+1}}{n} (C)^n \int_0^\infty (1 + \gamma_p)^{-n} f_{\gamma_p}(\gamma_p) d\gamma_p. \tag{22}$$

Expression $(1 + \gamma_p)^{-n}$ in (22) can be represented in terms of Fox's H-Function using relation ([25], Equation (1.7.3)) as

$$(1 + \gamma_p)^{-n} = \frac{1}{\Gamma(n)} H_{1,1}^{1,1}\left[\gamma_p \middle| \begin{array}{c} (1-n,1) \\ (0,1) \end{array}\right]. \tag{23}$$

Substituting (13) and (23) in (22), I_2 becomes

$$I_2 = \frac{\left(\frac{m_0}{\overline{\gamma}_p}\right)}{\ln(2)\Gamma(m_0)} \sum_{n=1}^\infty \frac{(-1)^{n+1}}{n\,\Gamma(n)} (C)^n$$

$$\times \int_0^\infty H_{1,1}^{1,1}\left[\gamma_p \middle| \begin{array}{c} (1-n,1) \\ (0,1) \end{array}\right]$$

$$\times H_{0,1}^{1,0}\left[\frac{m_0\gamma_p}{\overline{\gamma}_p} \middle| \begin{array}{c} \overline{} \\ (m_0-1,1) \end{array}\right] d\gamma_p. \tag{24}$$

The integral in (24) can be evaluated using ([25], Equation (2.6.8)) and further simplified using identities ([25], Equations (1.2.4) and (1.7.1)) to yield

$$I_2 = \frac{1}{\ln(2)\Gamma(m_0)} \sum_{n=1}^{\infty} \frac{(-1)^{n+1}}{n\,\Gamma(n)} (C)^n$$
$$\times G_{1,2}^{2,1} \left(\frac{m_0}{\overline{\gamma}_p} \,\middle|\, \begin{matrix} 1 \\ m_0, n \end{matrix} \right). \tag{25}$$

Substituting the values of I_1 and I_2 in (19), we obtain

$$I = \frac{1}{\ln(2)\Gamma(m_0)} G_{3,2}^{1,3} \left(\frac{\overline{\gamma}_p}{m_0} \,\middle|\, \begin{matrix} 1,\, 1,\, 1-m_0 \\ 1,\, 0 \end{matrix} \right)$$
$$+ \frac{1}{\ln(2)\Gamma(m_0)} \sum_{n=1}^{\infty} \frac{(-1)^{n+1}}{n\,\Gamma(n)} (C)^n$$
$$\times G_{1,2}^{2,1} \left(\frac{m_0}{\overline{\gamma}_p} \,\middle|\, \begin{matrix} 1 \\ m_0, n \end{matrix} \right). \tag{26}$$

It can be observed from (26) that our analytical approach has led us to an easily computable expression consisting of a summation and two Meijer's G-functions. Now, substituting the value of I in (17), we have

$$\bar{R}_p^{\text{NOMA}} = \frac{1}{2\ln(2)\Gamma(m_0)} G_{3,2}^{1,3} \left(\frac{\overline{\gamma}_p}{m_0} \,\middle|\, \begin{matrix} 1,\, 1,\, 1-m_0 \\ 1,\, 0 \end{matrix} \right)$$
$$\times \int_0^{\infty} f_{\gamma_s}(\gamma_s) d\gamma_s$$
$$+ \frac{1}{2\ln(2)\Gamma(m_0)} \sum_{n=1}^{\infty} \frac{(-1)^{n+1}}{n\,\Gamma(n)} \left(\frac{\alpha_0}{\alpha} \right)^n$$
$$\times G_{1,2}^{2,1} \left(\frac{m_0}{\overline{\gamma}_p} \,\middle|\, \begin{matrix} 1 \\ m_0, n \end{matrix} \right)$$
$$\times \underbrace{\int_0^{\infty} \left(\frac{\alpha\,\gamma_s}{\alpha\,\gamma_s + 1} \right)^n f_{\gamma_s}(\gamma_s) d\gamma_s}_{I_3}. \tag{27}$$

It is a well-known fact in statistics that $\int_0^{\infty} f_{\gamma_s}(\gamma_s) d\gamma_s = 1$. Furthermore, the expression $\left(\frac{\alpha\,\gamma_s}{\alpha\,\gamma_s + 1} \right)^n$ in I_3 can be written in terms of Fox's H-function using ([25], Equations (1.7.3) and (1.2.4)) as

$$\left(\frac{\alpha\,\gamma_s}{\alpha\,\gamma_s + 1} \right)^n = \frac{1}{\Gamma(n)} H_{1,1}^{1,1} \left[\alpha\,\gamma_s \,\middle|\, \begin{matrix} (1,1) \\ (n,1) \end{matrix} \right]. \tag{28}$$

We now focus on evaluating I_3 by substituting (13) and (28) in it to obtain

$$I_3 = \frac{\left(\frac{m_2}{\overline{\gamma}_s} \right)}{\Gamma(n)\Gamma(m_2)} \int_0^{\infty} H_{1,1}^{1,1} \left[\alpha\,\gamma_s \,\middle|\, \begin{matrix} (1,1) \\ (n,1) \end{matrix} \right]$$
$$\times H_{0,1}^{1,0} \left[\frac{m_2\gamma_s}{\overline{\gamma}_s} \,\middle|\, \begin{matrix} \overline{} \\ (m_2-1,1) \end{matrix} \right] d\gamma_s, \tag{29}$$

where m_2 is the fading severity parameter for the ST-PR link. Substituting $\alpha\,\gamma_s = x$, I_3 simplifies into

$$I_3 = \frac{\left(\frac{m_2}{\alpha\,\overline{\gamma}_s}\right)}{\Gamma(n)\Gamma(m_2)} \int_0^\infty H_{1,1}^{1,1}\left[x \,\middle|\, \begin{matrix}(1,1)\\(n,1)\end{matrix}\right]$$
$$\times H_{0,1}^{1,0}\left[\frac{m_2\,x}{\alpha\,\overline{\gamma}_s} \,\middle|\, \begin{matrix}\overline{\hspace{1.5cm}}\\(m_2-1,1)\end{matrix}\right]\, dx. \tag{30}$$

Integral I_3 can be evaluated using ([25], Equation (2.6.8)); then, using relation ([25], Equation (1.2.4)), we obtain

$$I_3 = \frac{1}{\Gamma(n)\Gamma(m_2)} H_{1,2}^{2,1}\left[\frac{m_2}{\alpha\,\overline{\gamma}_s} \,\middle|\, \begin{matrix}(1-n,1)\\(m_2,1),(0,1)\end{matrix}\right]. \tag{31}$$

A simplified expression of I_3 is obtained in terms of Meijer's G-function using ([25], Equation (1.7.1)) as

$$I_3 = \frac{1}{\Gamma(n)\Gamma(m_2)} G_{1,2}^{2,1}\left(\frac{m_2}{\alpha\,\overline{\gamma}_s} \,\middle|\, \begin{matrix}1-n\\m_2,0\end{matrix}\right). \tag{32}$$

The ergodic achievable rate expression at the PR after substituting the value of I_3 in (27) can be expressed as

$$\bar{R}_p^{\text{NOMA}} = \frac{1}{2\ln(2)\Gamma(m_0)} G_{3,2}^{1,3}\left(\frac{\overline{\gamma}_p}{m_0} \,\middle|\, \begin{matrix}1,\,1,\,1-m_0\\1,\,0\end{matrix}\right)$$
$$+ \frac{1}{2\ln(2)\Gamma(m_0)\Gamma(m_2)} \sum_{n=1}^\infty \frac{(-1)^{n+1}}{n\,\Gamma(n)\Gamma(n)}\left(\frac{\alpha_0}{\alpha}\right)^n$$
$$\times G_{1,2}^{2,1}\left(\frac{m_0}{\overline{\gamma}_p} \,\middle|\, \begin{matrix}1\\m_0,n\end{matrix}\right) G_{1,2}^{2,1}\left(\frac{m_2}{\alpha\,\overline{\gamma}_s} \,\middle|\, \begin{matrix}1-n\\m_2,0\end{matrix}\right). \tag{33}$$

Expression (33) contains two Meijer's G-functions inside the summation, which may cause slower convergence of the above expression. Therefore, it is more useful to replace Meijer's G-functions in terms of Tricomi confluent hypergeometric functions ([23], Equation (9.211.4)) using identity [27] for rapid convergence of the summation. Finally, we obtain a closed-form expression of the ergodic achievable rate at the PR as

$$\bar{R}_p^{\text{NOMA}} = \frac{1}{2\ln(2)\Gamma(m_0)} G_{3,2}^{1,3}\left(\frac{\overline{\gamma}_p}{m_0} \,\middle|\, \begin{matrix}1,\,1,\,1-m_0\\1,\,0\end{matrix}\right)$$
$$+ \frac{\left(\frac{m_0}{\overline{\gamma}_p}\right)^{m_0}\left(\frac{m_2}{\alpha\,\overline{\gamma}_s}\right)^{m_2}}{2\ln(2)\Gamma(m_2)} \sum_{n=1}^\infty \frac{(-1)^{n+1}}{n}\left(\frac{\alpha_0}{\alpha}\right)^n \Gamma(m_2+n)$$
$$\times \Psi\left(m_0, 1+m_0-n, \frac{m_0}{\overline{\gamma}_p}\right) \Psi\left(m_2+n, 1+m_2, \frac{m_2}{\alpha\,\overline{\gamma}_s}\right). \tag{34}$$

It is important to mention here that only two or three terms are sufficient for the convergence of the infinite series in (34).

Ergodic Achievable Rate at the SR: Using (7), the ergodic achievable data rate at the kth SR can be determined using (13) and (15) in (14) as

$$\bar{R}_{s,k}^{\text{NOMA}} = \mathbb{E}\{R_{s,k}^{\text{NOMA}}\}$$

$$= \frac{\left(\frac{m_{22}}{\overline{\gamma}_{sk}}\right)}{2\ln(2)\Gamma(m_{22})} \int_0^\infty H_{2,2}^{1,2}\left[\frac{\gamma_{sk}\,\alpha_k}{\gamma_{sk}\,\alpha+1}\,\middle|\,\begin{array}{c}(1,1),(1,1)\\(1,1),(0,1)\end{array}\right]$$

$$\times H_{0,1}^{1,0}\left[\frac{m_{22}\gamma_{sk}}{\overline{\gamma}_{sk}}\,\middle|\,\begin{array}{c}\overline{\phantom{(m_{22}-1,1)}}\\(m_{22}-1,1)\end{array}\right]d\gamma_{sk}, \tag{35}$$

where m_{22} is the fading severity parameter of the link between ST and the kth SR link and where $\gamma_{sk} = \rho_s|g_{s,k}|^2$, $\overline{\gamma}_{sk} = \mathbb{E}\{\gamma_{sk}\}$, and $\tilde{\alpha} = \sum_{i=k+1}^{K}\alpha_i$. Now, using the definition of Fox's H-function ([25], Equation (1.1.1)), expression (35) becomes

$$\bar{R}_{s,k}^{\text{NOMA}} = \frac{\left(\frac{m_{22}}{\overline{\gamma}_{sk}}\right)}{2\ln(2)\Gamma(m_{22})}\frac{1}{(2\pi\iota)^2}\int_{\mathfrak{L}_1}\int_{\mathfrak{L}_2}\frac{\Gamma(1+s)\Gamma(-s)^2}{\Gamma(1-s)}$$

$$\times \Gamma(m_{22}-1+t)(\alpha_k)^{-s}\left(\frac{m_{22}}{\overline{\gamma}_{sk}}\right)^{-t}\underbrace{\int_0^\infty \gamma_{sk}^{-s-t}(\gamma_{sk}\tilde{\alpha}+1)^s d\gamma_{sk}}_{I_4}$$

$$ds\,dt \tag{36}$$

where $\mathfrak{L}_1$ and $\mathfrak{L}_2$ are contours of the s- and t-complex planes, respectively. Now, integral I_4 can be evaluated using ([23], Equations (3.194.3) and (8.384.1)), yielding

$$I_4 = (\tilde{\alpha})^{-1+s+t}\frac{\Gamma(1-s-t)\Gamma(-1+t)}{\Gamma(-s)}, \tag{37}$$

where $Re\{t\} > 1 > Re\{s+t\}$. Substituting I_4 in (36), we obtain

$$\bar{R}_{s,k}^{\text{NOMA}} = \frac{\left(\frac{m_{22}}{\tilde{\alpha}\,\overline{\gamma}_{sk}}\right)}{2\ln(2)\Gamma(m_{22})}\frac{1}{(2\pi\iota)^2}\int_{\mathfrak{L}_1}\int_{\mathfrak{L}_2}\frac{\Gamma(1+s)\Gamma(-s)^2}{\Gamma(1-s)}$$

$$\times \Gamma(m_{22}-1+t)\Gamma(-1+t)\Gamma(1-s-t)$$

$$\times \left(\frac{\alpha_k}{\tilde{\alpha}}\right)^{-s}\left(\frac{m_{22}}{\tilde{\alpha}\,\overline{\gamma}_{sk}}\right)^{-t}ds\,dt. \tag{38}$$

It is now convenient to represent the above expression in terms of a bivariate Fox's H-function $H_{E,(A:C),F,(B:D)}^{L,N,N_1,M,M_1}[\cdot]$ as ([25], Equation (2.2.1))

$$\bar{R}_{s,k}^{\text{NOMA}} = \frac{\left(\frac{m_{22}}{\tilde{\alpha}\,\overline{\gamma}_{sk}}\right)}{2\ln(2)\Gamma(m_{22})}$$

$$\times H_{1,(0;0),0,(2:2)}^{1,1,0,1,2}\left[\begin{array}{c}\frac{\alpha_k}{\tilde{\alpha}}\\[2mm]\frac{m_{22}}{\tilde{\alpha}\,\overline{\gamma}_{sk}}\end{array}\,\middle|\,\begin{array}{c}(1,1)\\(1,1);\overline{}\\(1,1),(0,1)(-1,1),(m_{22}-1,1)\end{array}\right]. \tag{39}$$

The bivariate Fox's H-function reduces to a bivariate Meijer's G-function using relation ([25], Equation (2.3.1)). The bivariate Fox's H-function is a function of two variables that encompass almost all special functions of two variables, e.g., Meijer's G-function, MacRobert's E-function, Appell's function, and Whittaker function of two variables [25].

$$\bar{R}_{s,k}^{\text{NOMA}} = \frac{\left(\frac{m_{22}}{\bar{\alpha}\,\overline{\gamma}_{sk}}\right)}{2\ln(2)\Gamma(m_{22})}$$

$$\times \; G_{1,(0;0),0,(2:2)}^{1,1,0,1,2}\left(\begin{array}{c}\frac{\alpha_k}{\bar{\alpha}} \\[2mm] \frac{m_{22}}{\bar{\alpha}\,\overline{\gamma}_{sk}}\end{array}\;\middle|\;\begin{array}{c} 1;\frac{1}{\rule{1cm}{0.4pt}} \\[2mm] 1,0;-1,m_{22}-1\end{array}\right). \tag{40}$$

The bivariate Meijer's G-function can be evaluated by expressing it in the form of double Mellin–Barnes-type integrals by selecting suitable contours in the complex planes.

For the kth SR having an instantaneous rate given by (8), we follow the same steps using (20) and (21) to obtain the ergodic achievable rate $\bar{R}_{s,K}^{\text{NOMA}} = \mathbb{E}\{R_{s,K}^{\text{NOMA}}\}$ as

$$\bar{R}_{s,K}^{\text{NOMA}} = \frac{1}{\ln(2)\Gamma(m_{22})}G_{3,2}^{1,3}\left(\frac{\overline{\gamma}_{sk}}{m_{22}}\;\middle|\;\begin{array}{c}1,\,1,\,1-m_{22}\\1,\,0\end{array}\right). \tag{41}$$

Ergodic Achievable Rate at the PR when ST is silent: The ergodic achievable data rate at the PR, denoted by $\bar{R}_p^{\text{ST-silent}} = \mathbb{E}\{R_p^{\text{ST-silent}}\}$, during the silent mode can be determined using (9) and following the same steps using (20) and (21) to obtain

$$\bar{R}_p^{\text{ST-silent}} = \frac{1}{\ln(2)\Gamma(m_0)}G_{3,2}^{1,3}\left(\frac{\overline{\gamma}_p}{m_0}\;\middle|\;\begin{array}{c}1,\,1,\,1-m_0\\1,\,0\end{array}\right). \tag{42}$$

Note that when the ST is silent, we have $R_{s,k}^{\text{ST-silent}} = 0 \;\forall k$.

5. Results and Discussion

In this section, we present numerical results to validate the ergodic achievable rate analysis carried out in Section 3. We compare the derived analytical results with the simulation's results. Here, the outage probabilities of PR and SRs (given in [7]) are also incorporated in the results. Similarly to [7], we assume that $\mathbb{E}\{|h_p|^2\} = \mathbb{E}\{|h_{s,k}|^2\} = 0.1$ and $\mathbb{E}\{|h_s|^2\} = \mathbb{E}\{|g_p|^2\} = \mathbb{E}\{|g_{s,k}|^2\} = 0.2$. The fading severity for all channels is set to $m_0 = m_2 = m_{22} = 2$. The simulation results are obtained by averaging over one million independent channel realizations.

Figure 2 shows the ergodic achievable rate of the system (including PR and SRs) against various values of transmit SNR, where $\rho_p = \rho_s$. We also plot the ergodic achievable rate of the PR and the ergodic achievable sum rate of SRs. Here, we assume that $K = 2$, $\alpha_1 = 0.6$, $\alpha_2 = 0.3$, and $\alpha_3 = 0.1$, and the minimum rate requirements are set to $R_0 = R_1 = R_2 = 0.5$ for this set of simulation. It is observed that the analytical ergodic achievable rate's results exactly match the simulation's results, thus validating the analytical analysis carried out in Section III. Moreover, it can be observed that the ergodic achievable rate increases with the increasing values of ρ_p and ρ_s. Additionally, we see that the PR has a higher attainable rate than the SR, which is expected for CR as PR is the only licensed entity among all communicating nodes. Furthermore, for the values of $\rho_p < 10$ dB, it can be seen that the ergodic achievable rate is almost equivalent to zero. This is a result of the CRN's inability to satisfy the PR's minimum rate requirements for transmit power values below a certain threshold. If so, no CRN-based transmission will take place; instead, the PR will send its information directly to the destination without involving the SRs. We exclusively display the outcomes for the case where CRN is employed in Figure 2.
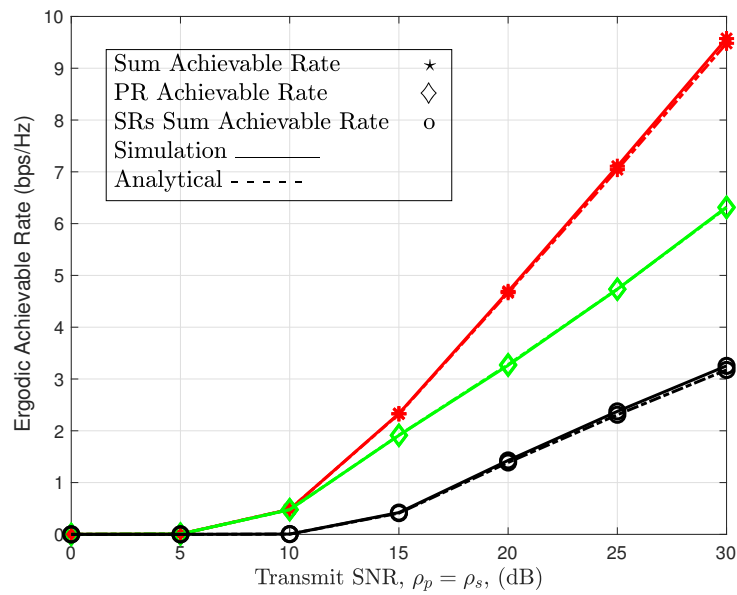
Figure 2. Ergodic achievable rate performance versus transmit SNR.

By fixing the values of ρ_p and ρ_s to 20 dB in Figure 3, we offer findings for the system's ergodic attainable rate against different values of the Nakagami-m fading parameter for the same setup in Figure 2. We can see that the formulas hold for the non-integer values of m, and the results show that the analytical and simulation findings are identical. Our analytical findings are equally valid in the case where $m < 1$, which is worst than the Rayleigh fading scenario. This graph depicts the range of our results and their applicability to all potential m values. Additionally, we can see that the achievable rate rises as the Nakagami-m parameter's value rises. Furthermore, we can see that the PR's achievable rate is roughly twice as high as the sum rate of all SRs overall, satisfying the PR rate's guaranteed conditions set forth by the CRN.
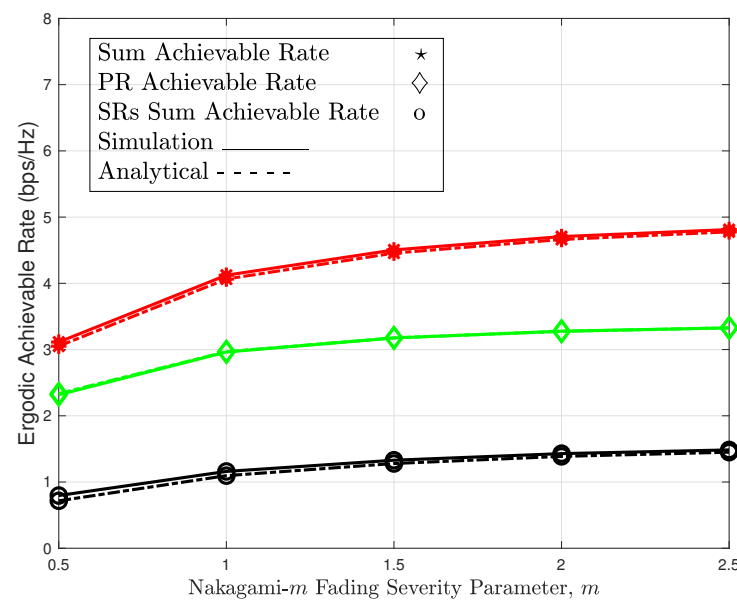

Figure 3. Ergodic achievable rate performance versus Nakagami-m fading severity parameter.

On the same grounds in Figure 4, the ergodic achievable rates are plotted against different values of α_0 with $K = 2$ and $R_0 = R_1 = R_2 = 0.5$. Here, we set $\alpha_1 = ((1 - \alpha_0)/2) + 0.025$ and $\alpha_2 = ((1 - \alpha_0)/2) - 0.025$. It can be seen that as the value of α_0 increases, the ergodic achievable sum rate of SRs decreases slightly because more power is allocated to the PR;

hence, less power will be allocated to the SRs. Again, it can be observed that the derived analytical results are consistent with the simulation's results.
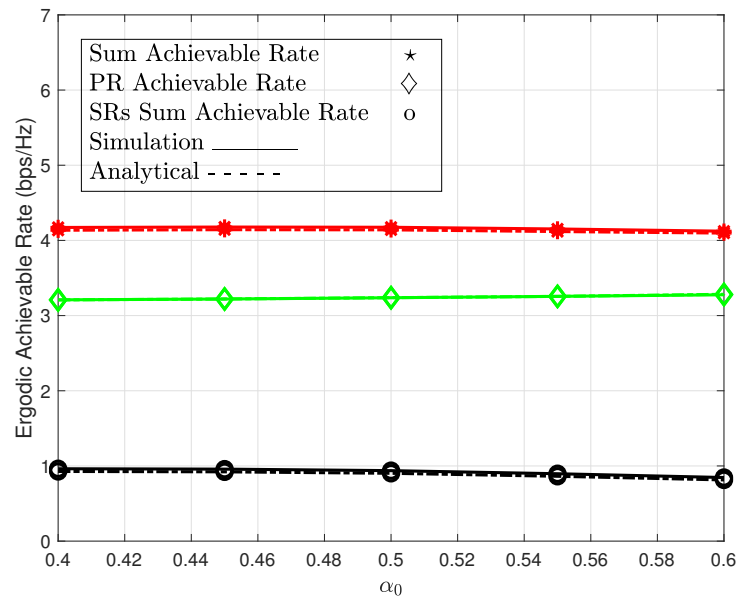

Figure 4. Ergodic achievable rate performance against different values of α_0.

Finally, we plot the ergodic achievable rates for different values of K (i.e., the number of SRs in the network) in Figure 5, where $\rho_p = \rho_s = 10$ dB, $R_0 = 0.5$, and $R_1 \cdots R_K = 0.05$. We set the value of α_0 to 0.5. For α_1 to α_K, we take K equally spaced points between 1 to 0.5 and normalize them such that their sum is equal to 0.5. It can be seen that as we increase the number of SRs in the network, the ergodic achievable sum rate of SRs increases initially but then saturates to a fixed value. Moreover, there is a small gap between the analytical and simulation results in SR's achievable sum rate. This slight difference is a result of the use of approximate outage probability values derived in [7] for SRs.
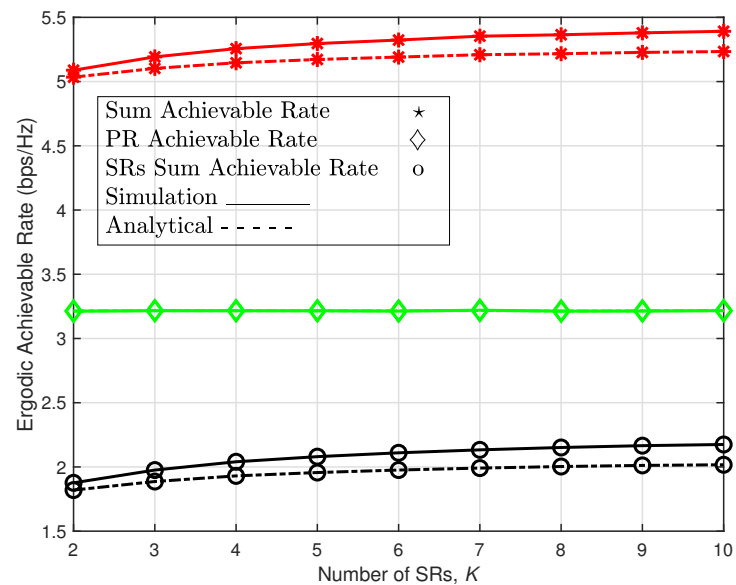

Figure 5. Ergodic achievable rate performance versus the number of SRs, K.

6. Conclusions

We derived ergodic achievable rate expressions at the PR and SRs for the NOMA-based cooperative spectrum-sharing CRN. In this paper, we assumed that communication channels experience Nakagami-m fading. The analysis presented can be used for both

integer and non-integer fading index values. We compare the results of the derived ergodic achievable rate expressions with the numerically computed achievable rate results. The derived ergodic achievable rate's results match well with the simulation's results.

The analysis presented in this study will be useful in predicting the performance of the NOMA-based spectrum-sharing CRN in Nakagami-*m* fading channels, where fading severity parameter *m* can be varied to any integer and non-integer value. In future work, the statistical performance of NOMA-based spectrum-sharing CRNs can be characterized in the presence of intelligent reflecting surfaces (IRSs), which can be useful when direct transmission links between communicating nodes are blocked. The deployment of IRSs can also be utilized to improve the received signal strength in NOMA-based CRNs.

Author Contributions: This article was prepared via the collective efforts of all authors. Conceptualization, S.H.A., B.A., J.M., A.K., M.A.J., J.A. and N.H.; critical review, S.H.A., B.A., J.M., A.K., M.A.J., J.A. and N.H.; writing—original draft, S.H.A., B.A. and J.M.; writing—review and editing, A.K., M.A.J., J.A. and N.H. All authors have read and agreed to the published version of the manuscript.

Institutional Review Board Statement: Not applicable.

Informed Consent Statement: Not applicable.

Data Availability Statement: Data will be available on request from the corresponding author.

Conflicts of Interest: The authors declare no conflicts of interest.

References

1. Qian, B.; Zhou, H.; Ma, T.; Yu, K.; Yu, Q.; Shen, X. Multi-Operator Spectrum Sharing for Massive IoT Coexisting in 5G/B5G Wireless Networks. *IEEE J. Sel. Areas Commun.* **2021**, *39*, 881 – 895. [CrossRef]
2. Chatterjee, S.; Mukherjee, R.; Ghosh, S.; Ghosh, D.; Ghosh, S.; Mukherjee, A. Internet of Things and cognitive radio—Issues and challenges. In Proceedings of the 2017 4th International Conference on Opto-Electronics and Applied Optics (Optronix), Kolkata, India, 2–3 November 2017; pp. 1–4. [CrossRef]
3. Mukherjee, A.; Rodrigues, J.J.P.C.; Goswami, P.; Manman, L.; Hazra, R.; Yang, L. Green Cooperative Communication Based Cognitive Radio Sensor Networks for IoT Applications. In Proceedings of the 2020 IEEE International Conference on Communications Workshops (ICC Workshops), Dublin, Ireland, 7–11 June 2020; pp. 1–6. [CrossRef]
4. Lv, L.; Chen, J.; Ni, Q.; Ding, Z.; Jiang, H. Cognitive Non-Orthogonal Multiple Access with Cooperative Relaying: A New Wireless Frontier for 5G Spectrum Sharing. *IEEE Commun. Mag.* **2018**, *56*, 188–195. [CrossRef]
5. Ding, Z.; Peng, M.; Poor, H.V. Cooperative Non-Orthogonal Multiple Access in 5G Systems. *IEEE Commun. Lett.* **2015**, *19*, 1462–1465. [CrossRef]
6. Zhang, Z.; Ma, Z.; Xiao, M.; Ding, Z.; Fan, P. Full-Duplex Device-to-Device-Aided Cooperative Nonorthogonal Multiple Access. *IEEE Trans. Veh. Technol.* **2017**, *66*, 4467–4471. [CrossRef]
7. Lv, L.; Ni, Q.; Ding, Z.; Chen, J. Application of Non-Orthogonal Multiple Access in Cooperative Spectrum-Sharing Networks Over Nakagami-*m* Fading Channels. *IEEE Trans. Veh. Technol.* **2017**, *66*, 5506–5511. [CrossRef]
8. Haykin, S. Cognitive radio: Brain-empowered wireless communications. *IEEE J. Sel. Areas Commun.* **2005**, *23*, 201–220. [CrossRef]
9. Kumar, V.; Cardiff, B.; Flanagan, M.F. Fundamental Limits of Spectrum Sharing for NOMA-Based Cooperative Relaying. In Proceedings of the 2018 IEEE Globecom Workshops (GC Wkshps), Abu Dhabi, United Arab Emirates, 9–13 December 2018; pp. 1–7. [CrossRef]
10. Kumar, V.; Cardiff, B.; Flanagan, M.F. Fundamental Limits of Spectrum Sharing for NOMA-Based Cooperative Relaying Under a Peak Interference Constraint. *IEEE Trans. Commun.* **2019**, *67*, 8233–8246. [CrossRef]
11. Chu, Y.; Champagne, B.; Zhu, W.P. NOMA-based cooperative relaying for secondary transmission in cognitive radio networks. *IET Commun.* **2019**, *13*, 1840–1851. [CrossRef]
12. Hakimi, A.; Mohammadi, M.; Mobini, Z. Outage Probability of Wireless-powered Multi-antenna Cooperative Spectrum Sharing Networks with Full-duplex and NOMA Transmissions. In Proceedings of the 2018 9th International Symposium on Telecommunications (IST), Tehran, Iran, 17–19 December 2018; pp. 127–132. [CrossRef]
13. Kumar, V.; Ding, Z.; Flanagan, M.F. On the Effective Rate of NOMA in Underlay Spectrum Sharing. *IEEE Trans. Veh. Technol.* **2021**, *70*, 12220–12225. [CrossRef]
14. Lv, L.; Chen, J.; Ni, Q.; Ding, Z. Design of Cooperative Non-Orthogonal Multicast Cognitive Multiple Access for 5G Systems: User Scheduling and Performance Analysis. *IEEE Trans. Commun.* **2017**, *65*, 2641–2656. [CrossRef]

15. Do, D.T.; Le, A.T.; Lee, B.M. On Performance Analysis of Underlay Cognitive Radio-Aware Hybrid OMA/NOMA Networks with Imperfect CSI. *Electronics* **2019**, *8*, 819. [CrossRef]
16. Arzykulov, S.; Nauryzbayev, G.; Tsiftsis, T.A.; Maham, B.; Abdallah, M. On the Outage of Underlay CR-NOMA Networks With Detect-and-Forward Relaying. *IEEE Trans. Cogn. Commun. Netw.* **2019**, *5*, 795–804. [CrossRef]
17. Zhang, X.; Zhang, B.; An, K.; Chen, Z.; Xie, S.; Wang, H.; Wang, L.; Guo, D. Outage Performance of NOMA-Based Cognitive Hybrid Satellite-Terrestrial Overlay Networks by Amplify-and-Forward Protocols. *IEEE Access* **2019**, *7*, 85372–85381. [CrossRef]
18. Liu, X.; Wang, X. Outage probability and capacity analysis of the collaborative NOMA assisted relaying system in 5G. In Proceedings of the IEEE/CIC International Conference on Communications in China (ICCC), Chengdu, China, 27–29 July 2016; pp. 1–5. [CrossRef]
19. So, J.; Sung, Y. Improving Non-Orthogonal Multiple Access by Forming Relaying Broadcast Channels. *IEEE Commun. Lett.* **2016**, *20*, 1816–1819. [CrossRef]
20. Zhang, L.; Liu, J.; Xiao, M.; Wu, G.; Liang, Y.C.; Li, S. Performance Analysis and Optimization in Downlink NOMA Systems With Cooperative Full-Duplex Relaying. *IEEE J. Sel. Areas Commun.* **2017**, *35*, 2398–2412. [CrossRef]
21. Dhanasekaran, S.; Sushma, T.R. Performance Analysis of Cell-Center Users in NOMA Based-Spectrum Sharing Protocol. *IEEE Commun. Lett.* **2020**, *24*, 52–56. [CrossRef]
22. Molisch, A.F. *Wireless Communications*, 2nd ed.; Wiley-IEEE Press: Chichester, UK, 2011.
23. Gradshteyn, I.S.; Ryzhik, I.M. *Table of Integrals, Series and Products*, 7th ed.; Academic Press: Burlington, MA, USA, 2007.
24. Alvi, S.H.; Wyne, S.; da Costa, D.B. Performance analysis of dual-hop AF relaying over α-μ fading channels. *AEU Int. J. Electron. Commun.* **2019**, *108*, 221–225. [CrossRef]
25. Mathai, A.M.; Saxena, R.K. *The H-Function with Applications in Statistics and Other Disciplines*; John Wiley & Sons: New York, NY, USA, 1978.
26. Cook, I.D. The H-Function and Probability Density Functions of Certain Algebraic Combinations of Independent Random Variables with H-Function Probability Distribution. Ph.D. Thesis, U.T. Austin, Austin, TX, USA, 1981.
27. Weisstein, E.W. Hypergeometric Functions and MeijerG. Available online: https://functions.wolfram.com/HypergeometricFunctions/MeijerG (accessed on 10 August 2022).